Investigation into Durable Polymers with Enhanced Toughness and Elasticity for Application in Flexible Li-ion Batteries

Craig A. Jenkins,* Stuart R. Coles, Melanie. J. Loveridge

WMG, University of Warwick, 6 Lord Bhattacharyya Way, Coventry, CV4 7AL

ABSTRACT: Next-generation wearable devices compel the development of lithium-ion batteries (LIBs) which can afford mechanical flexibility, whilst remaining safe and stable energy sources. In conventional battery designs the electrode coatings are susceptible to fracture and disintegration when exposed to cyclic flexure. This results in capacity loss, resistance increases and severely limits their cycle life. Polyurethane (PU) has been investigated as a battery binder but without research into the variety of chemistries available, and how they affect performance. This research investigates three different PU chemistries, each composed of a different polyol backbone – polyester, polyether and polycaprolactone. These are compared with PVDF, the most commonly used rigid binder in industry. The combination of electrochemical and mechanical characterisation identified the importance of PU binder chemistry, particularly when the binder's interaction with the electrolyte was considered. Both the polyester and polycaprolactone PU chemistries swelled significantly when placed in an electrolyte, compromising their conductive networks and mechanical advantages. In contrast, polyether PU was found to be a suitable binder for flexible batteries as it has strong adhesion and retains its properties even after swelling in the electrolyte. These findings present a promising polymer choice to facilitate the development of advanced and durable electrodes for flexible energy storage systems.

KEYWORDS: *Electrochemistry, polymer binder, flexible battery, lithium-ion, polyurethane, AC Impedance, mechanical characterisation, electrode adhesion*

INTRODUCTION

The emergence of flexible electronics and wearable devices has generated a demand for portable energy sources that can provide power in a flexible form factor. LIBs are available in thin and energy-dense pouch formats but they consist of materials that are brittle and cannot accommodate strain.[1,2] When exposed to fatigue bending stresses, the strains induced in the cell layers cause the electrode coatings to crack and delaminate, resulting in capacity loss and an increase in internal resistance.[3,4]

The electrode coatings are composed of active material (energy storing) particles, conductive additives and a binder. The binder is essential in establishing and maintaining mechanical integrity of the electrode. It forms a conductive matrix with electronically conductive additives, binding active material particles together and securing them to the current collector.[5] Polyvinylidene fluoride (PVDF) is widely used due to its chemical resistance, stability over a wide voltage range and proven ability to utilise the high capacities of battery active materials.[6,7] However, PVDF is a brittle polymer with a structure that exhibits only weak Van der Waals interactions thus providing limited adhesion and making it unsuitable for flexible batteries.[8–10] Despite these flaws, there is a scarcity of research investigating alternatives that retain the chemical and voltage stability of PVDF yet provide enhanced adhesion and elasticity.

Polyurethane (PU) is suggested as having a good combination of properties for a flexible battery binder.[11] It is composed of hard domains that provide mechanical strength and soft domains that enable flexibility and elasticity. The combination of hydrogen bonding and dipole-dipole interactions enables good adhesion both between polymer chains and to the current collector and active materials.[12] Furthermore, PU's properties are highly tuneable by way of manipulating the proportions of these domains and selecting different chemical precursors. The latter has not been addressed by other researchers in the field. Studies investigate single chemistries of polyurethane, neglecting to optimise their parameters or investigate how the different chemistries might affect performance.[11,13,14] PU is also non-toxic and in contrast to PVDF it does not decompose into hydrogen fluoride (HF) upon combustion, which can be a hazard in the event of thermal runaway.[15]

Paramount to binder effectiveness is compatibility with the electrolyte solvents. The two must interact favourably in order to permit lithium ion flux through the electrode's bulk. However, the binder must not degrade or swell excessively, as this can compromise the battery's mechanical properties. The PU chemistries are generally dictated by their diol backbone, which can be polyester, polyether or polycaprolactone. There have been attempts to test the stability of PUs in various organic electrolyte solvents, with propylene carbonate (PC) demonstrating compatibility, but other common solvents experiencing dissolution.[13] However, the methods used are not clear, the diol backbone is not specified, with another key paper contradicting the conclusion that PU is soluble in ethylene carbonate/diethyl carbonate (EC/DEC), achieving good performance with the same solvent mixture.[14] Despite specifying the diol backbone as polyether, this second study is also questionable as the commercial PU is specified to be polyester-based on the supplier's website. A third group synthesised their own polyether PU and combined it with an EC/DMC solvent mixture (DMC = dimethyl carbonate).[11] This demonstrated reasonably good results but neither of the two previous papers investigated DMC as a solvent, hence their findings cannot be directly compared. To summarise, PU is a

promising binder for flexible batteries but the limited published research and non-aligned findings are inconclusive, requiring further progress.

Consequently, this research aims to extend and consolidate knowledge of PU binders in order to better understand how PU chemistry can affect binder performance and hence demonstrate its suitability for flexible batteries. Three commercial PU polymers were investigated as electrode binders, with PVDF serving as a baseline, and each PU consisting of a different diol – polyester, polyether and polycaprolactone. Their properties were characterised through a combination of mechanical and electrochemical methods. The formulation was also systematically developed so that the impact of inactive material proportions on adhesion and cyclic capacity retention could be investigated. For the purposes of direct and fair comparison with PVDF, a commercially relevant 90:5:5 formulation was used for the majority of testing. Future work beyond this study will investigate the impedance characteristics and mechanical durability of the optimised formulations.

EXPERIMENTAL SECTION

Electrode preparation. Electrodes formulated with polyvinylidene fluoride (PVDF) as the binder served as a baseline for electrochemical performance and fatigue flexing ability. To fabricate the electrodes a slurry consisting of an active material, a binder and a conductive additive was mixed together and coated onto a current collector. Baseline PVDF cathodes contained 90 wt% carbon-coated lithium iron phosphate (cc-LFP – BASF) active material, 5 wt% PVDF (PVDF 5130 – Solef SOLVAY) binder and 5 wt% C65 conductive additive (TIMCAL C-ENERGY Super C65 carbon black, Imerys). The PVDF binder was an 8 wt% solution in N-methyl-2-pyrrolidone (NMP, 97% Sigma Aldrich) dispersed overnight in a Turbula T2F shaker mixer. The dry materials, cc-LFP and C65, were dried overnight in an oven at 60 °C to minimise moisture content and combined in a THINKY ARE-250 planetary mixer for 30 minutes at 500 revolutions per minute (rpm). The binder solution and dry materials were then combined in the THINKY mixer with additional NMP added incrementally to adjust the viscosity. The viscosity was kept in the range 3-10 Pa s measured at a 10 s^{-1} shear rate. Higher viscosity avoids sedimentation and gives the slurry structure, enhancing stability. However, the slurry must be thin enough to flow and uniformly wet the substrate at the coating shear rates. The slurry was dispersed at 1500 rpm in 10-minute bursts for a minimum total dispersion time of 30 minutes.

Table 1. Physical properties of PU binders, as measured by suppliers.[16,17]

	Hardness, Shore A	Ultimate Elongation (%)	Density (g/cm3)	Tensile Strength (MPa)
Ester-PU	83	600	1.20	55
Caprolactone-PU	84	-	1.18	-
Ether-PU	96	500	1.15	55

For the PU binders the same procedure was followed except the binder solution was adjusted to 16 wt% PU in NMP. A higher polymer solids content ensured that the initial NMP in the mix was minimised and could be added incrementally for enhanced viscosity control. Three PU binders were selected, each consisting of a different base polyol: polyester (Elastollan 1195 A10 – BASF), polycaprolactone (430218, Sigma-Aldrich) and polyether (Elastollan B85 A10 – BASF). Elasticity and strength were targeted and all three binders had similar mechanical properties as shown in Table 1. The mixing procedure followed the same steps for all of the formulations.

The electrode slurries were coated onto aluminium foil (15 µm, MTI Corporation) using a draw-down coater (RK Instruments Ltd.) with a 150 µm fixed-blade applicator. The coated substrates were immediately transferred to a hot plate and dried at 80 °C. They were then transferred to a dry room (dew point of -45 °C) and dried overnight at 50 °C in a vacuum oven to ensure complete solvent and water removal prior to cell assembly. Calendered electrodes were pressed to 50% porosity on an 80 °C heated roller press (Tmax Battery Equipments) and dried overnight for a second time.

Electrochemical characterization. The electrodes were punched into 14.8 mm discs and assembled in a dry room into Hohsen CR2032 coin half-cells. Lithium foil served as the counter electrode and a polypropylene microporous membrane with a hydrophilic surfactant coating (Celgard 3501, 25 µm) was used as the separator. Cells were filled with one of two different PuriEL battery electrolytes (Soulbrain). Both electrolytes consisted of 1M $LiPF_6$ and 1 wt% VC dissolved in a solvent mixture, which for R&D 281 was 3:7 EC/EMC and for R&D 857 was 3:7 EC/DMC.

The cells were cycled between 2.5 V and 4 V in galvanostatic mode on a Maccor Series 4000 cycler, with a constant voltage step at the end of each charge cycle. The formation cycle was set at a C-rate of C/10, followed by 300 cycles at 1C for the long-term cycling measurements.

Potentiostatic Electrochemical Impedance Spectroscopy (PEIS) measurements were conducted on a VMP3 potentiostat (Bio-Logic). The same cycling procedure was used, C/10 formation and 1C long-term. An impedance spectrum was measured every 10 cycles. The spectrum was measured on the discharge cycle at 50% SOC after a 15 minute rest. The impedance measurements were taken at frequencies of 500 kHz to 10 mHz with 20 points per decade. The quality of the impedance data was verified by calculating the Kramers-Kronig residuals in Lin-KK software.

Mechanical characterization. Tensile testing was performed on an Instron 5982 100 kN static testing system fitted with a 1 kN load cell and an AVE 2 non-contacting video extensometer. Polymer films were prepared by solvent casting the polymer binder solutions (same concentrations as used in the electrode preparation) to a dry thickness of 0.2 ± 0.05 mm. The films were dried on a hot plate at 80 °C and then die-pressed into ASTM D638 Type V dog-bone specimens (width of 3.18 mm and gauge length of 25.4 mm). Specimens were secured with self-tightening grips, to prevent slippage at high strains, and strained at a crosshead speed of 50 mm min^{-1}. Measured load was divided by the specimen's original cross-sectional area to convert it to engineering stress. Strain was captured using the video extensometer but as some of the samples stretched beyond the viewing angles of the camera, the strain values had to be extrapolated. Young's modulus was calculated using a chord modulus fitted between 0.5% and 1.5% offset strain. Toughness was calculated by integrating the stress-strain curves in Excel.

A pull-off adhesion test was developed to measure and compare adhesion with binder content. It was preferred to a tape-peel test as the latter relies on manual tape application and the measured adhesion force is sensitive to the tape application force.[18] The

pull-off adhesion method involves compression and tension phases, with the entire sequence performed on a uniaxial tensile testing machine so that precise and repeatable forces are applied. Tesa 5696 double-sided tape was applied to the current collector side of the coating and then 19 mm diameter discs were punched out of the taped area. The discs were adhered to aluminium SEM stubs which had been prepared for adhesion by cleaning and degreasing with IPA. Smaller 12.8 mm diameter discs were punched out of double-sided tape, with release paper applied to the reverse to prevent them from sticking. The release paper was removed from one side and the discs were adhered to SEM stubs. A schematic of the complete stub, electrode and tape assembly is shown in Figure 1.

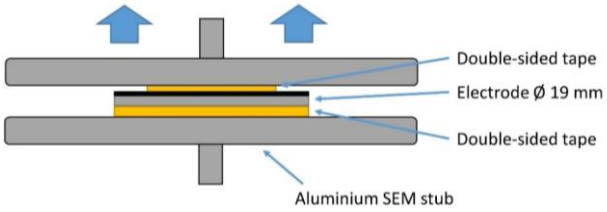

Figure 1. Schematic showing cross-sectional view of the electrode and double-sided tape sandwich prior to pull-off.

For each measurement a pair of stubs was loaded onto an Instron 8872 25 kN dynamic fatigue testing system fitted with custom-built grips that clamped onto the stubs' pins. Before running the test, a pre-compression of 150 kPa was applied for 10 s with the release paper still in place to ensure the tape was firmly and uniformly attached. The testing protocol initiated with a 600 kPa compression held for 60 s, followed by a 100 mm min-1 crosshead speed in a tensile direction in order to pull the material off the surface. The adhesion force was determined from the height of the peak that was measured during the pull-off phase. To capture these peaks the system was set to a data acquisition rate of 2 kHz. A higher sampling rate was necessary in order to resolve the very short time interval in which the adhesion peak occurred.

RESULTS AND DISCUSSION

Uniaxial tensile test. It was essential that the binders had sufficient elasticity to cope with the localised tensile stresses caused by flexure. The suppliers provided data on their mechanical properties, shown in Table 1. However, these would have been extruded or injection moulded specimens. Electrode coatings are solvent-cast so it was crucial to check whether their mechanical advantages were reproducible. Polymer specimens of each PU binder were solvent-cast and compared with PVDF.

Table 2. Ultimate elongation, toughness and Young's modulus of polymer binders with error defined as 95% confidence interval and a minimum of five specimens tested per polymer.

	Ultimate Elongation (%)	Young's modulus (MPa)	Toughness (J/cm3)
PVDF	11 ± 4	787 ± 178	1.7 ± 0.5
Ester-PU	739 ± 43	22.4 ± 3.9	91.7 ± 38.9
Caprolactone-PU	860 ± 39	20.3 ± 3.5	129 ± 22.6
Ether-PU	626 ± 16	67.6 ± 11.4	217 ± 21.1

The tensile data in Table 2 revealed that all three PU binders could be stretched to over 600% of their original length before failure, whereas PVDF could only be stretched to around 10%. Their tensile strengths and ultimate elongations were similar to those that were quoted by the manufacturers, demonstrating good reproducibility. The tensile strength of ether-PU outperformed the manufacturer's data (85 MPa compared to 55 MPa) suggesting that fewer defects were formed during solution casting.

From the inset in Figure 2, it can be seen that the PU binders initially exhibited a short linear region in their stress-strain curves which is typical of thermoplastic elastomers. This region describes the elastic (reversible) response before the yield point,

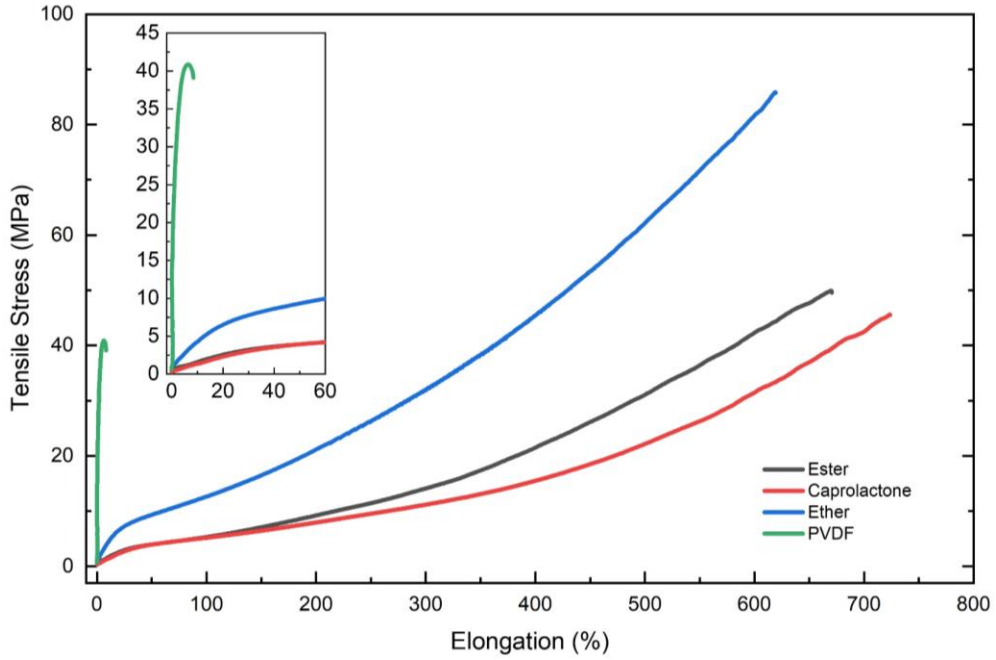

Figure 2. Stress-strain curves of polymer binders recorded on uniaxial tensile tested machine. Inset is zoomed portion of curve showing initial linear region of PU binders.

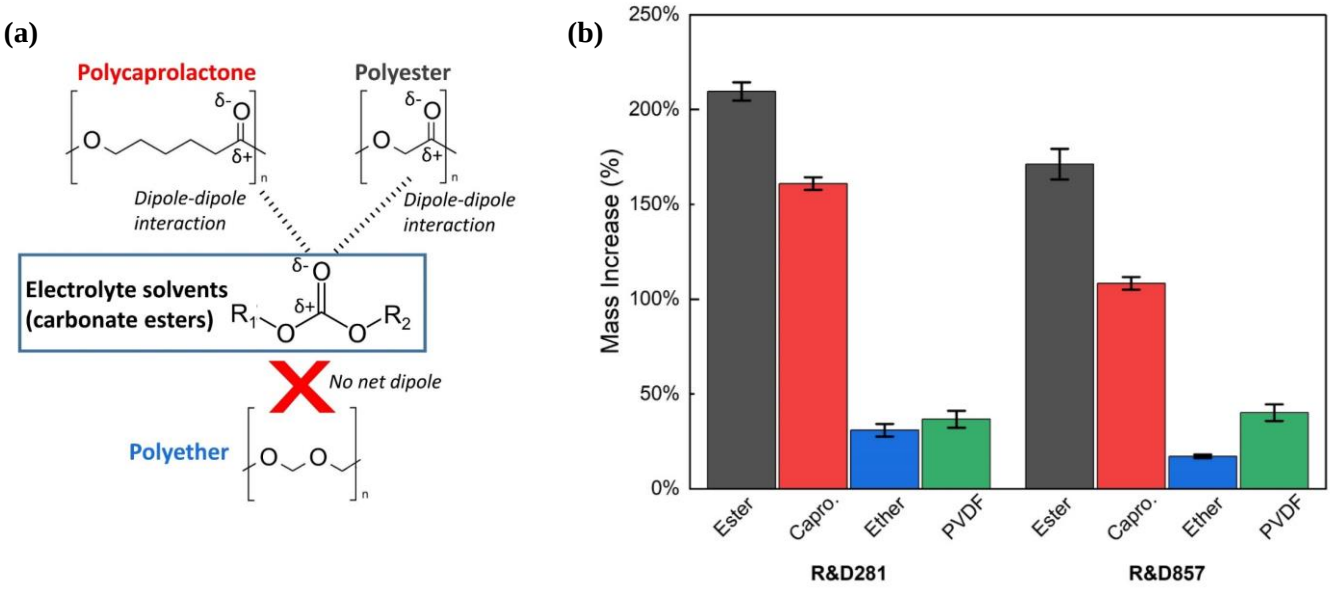

Figure 3. (a) Chemical structures of polyurethanes and electrolyte solvents. (b) Mass increase of the binders by swelling when soaked in electrolytes R&D281 and R&D857 for 3 days.

(permanent) deformation. Therefore, at elongations below 10% the deformation is entirely reversible. This is a significant improvement compared with PVDF, where the majority of specimens exhibited brittle failure before reaching 10% elongation. A flexible phone or watchband might experience a nominal strain of around 5% acting on its surfaces, which lies comfortably within the elastic limit of PU.[19]

Table 2 also displays the toughness and Young's modulus for each binder. The data shows that the modulus of PVDF is an order of magnitude higher than PU, which clearly makes it much more prone to brittle facture. The higher toughness of PU is desirable as it demonstrates how it can accommodate a greater amount of strain energy before failing. Ether-PU has the highest toughness, exceeding 200 J cm^{-3}, and although it is slightly stiffer than the other two PU binders, the small sacrifice in elasticity for enhanced durability could be beneficial.

In summary, all three PU binders were more elastic with a higher toughness than PVDF whilst retaining good strength. The favourable mechanical properties were obtained using conventional solvent-casting methods, so the binders can be implemented without the need for additional processing.

Polymer binder swelling. In order to establish the compatibility of the PU chemistries in battery electrolytes, swelling tests were carried out in two common solvent mixtures. Among the three types of PU tested, the ester-based and caprolactone-based chemistries swelled significantly more in the electrolyte solutions than the ether-based PU. They consistently increased in mass by over 100% compared with a 20-30% mass increase for the ether-PU (Figure 3b). The large differences in swelling is explained by examining the chemical structures of the solvents used in the electrolyte solutions. The electrolyte solvents are a mixture of linear chain carbonate esters and cyclic esters. R&D 281 electrolyte contains ethyl methyl carbonate (EMC) and R&D 857 contains dimethyl carbonate (DMC), as shown in Figure 3a, with ethylene carbonate (EC), a cyclic ester, common to both electrolytes. The ester group of these solvents induces a net dipole that interacts with the ester groups in the ester-PU and caprolactone-PU.[20] The ester-PU swells slightly more than the caprolactone-PU as it has a higher density of dipole-inducing groups due to their shorter chain length. The ether- PU does not have a net dipole and so interacts relatively weakly with the electrolyte solvents.

Cyclic electrochemical performance. The binders were tested in coin cells (half-cell configuration) using carbon-coated lithium iron phosphate (cc-LFP) as the cathode material. The results for the uncalendered electrodes are displayed in Figure 4a. The ether-PU binder reached a first cycle capacity of 150.7 mAh g^{-1} for a 0.1C charge and discharge, which is close to the theoretical maximum for cc-LFP (164 mAh g^{-1} for 3.6 wt% carbon coating). This was a marked improvement over the caprolactone-PU and ester-PU binders, which showed first cycle capacities of 130.7 mAh g^{-1} and 90.4 mAh g^{-1}, respectively. Before cycling began, all of the electrodes had a rest step of 8 hours at open circuit potential (OCV) to ensure that the polymer binders were approximately at their equilibrium swelling states. It is noticeable that the first cycle capacities followed the same trend as swelling degrees, whereby increased swelling correlated to reduced capacity. The ester-PU and caprolactone-PU also showed high voltage hysteresis and short voltage plateaus (see Figure S1 in the Supporting Information). Voltage hysteresis and reduced capacity are usually signs of poor electronic conductivity. The decrease in electronic conductivity upon binder swelling can be attributed to loss of electrical contact between neighbouring active particles and the current collector.[21,22] The vast area compared to the micron-sized thickness of the coating suppresses lateral expansion such that binder material deforms in a direction normal to the current collector surface as it swells. This causes a build-up of stress, with tensile forces acting on the top and bottom surfaces of particles and compressive forces acting against their sides. These stresses result in loss of electrical contact as the binder delaminates both from particle surfaces and the current collector.

To further investigate the link between swelling behaviour and loss of electronic conductivity, the electrodes were calendered to a porosity of 50%. Calendering enhances electronic conductivity by shortening conductive pathways, reducing porosity and increasing both particle/binder and

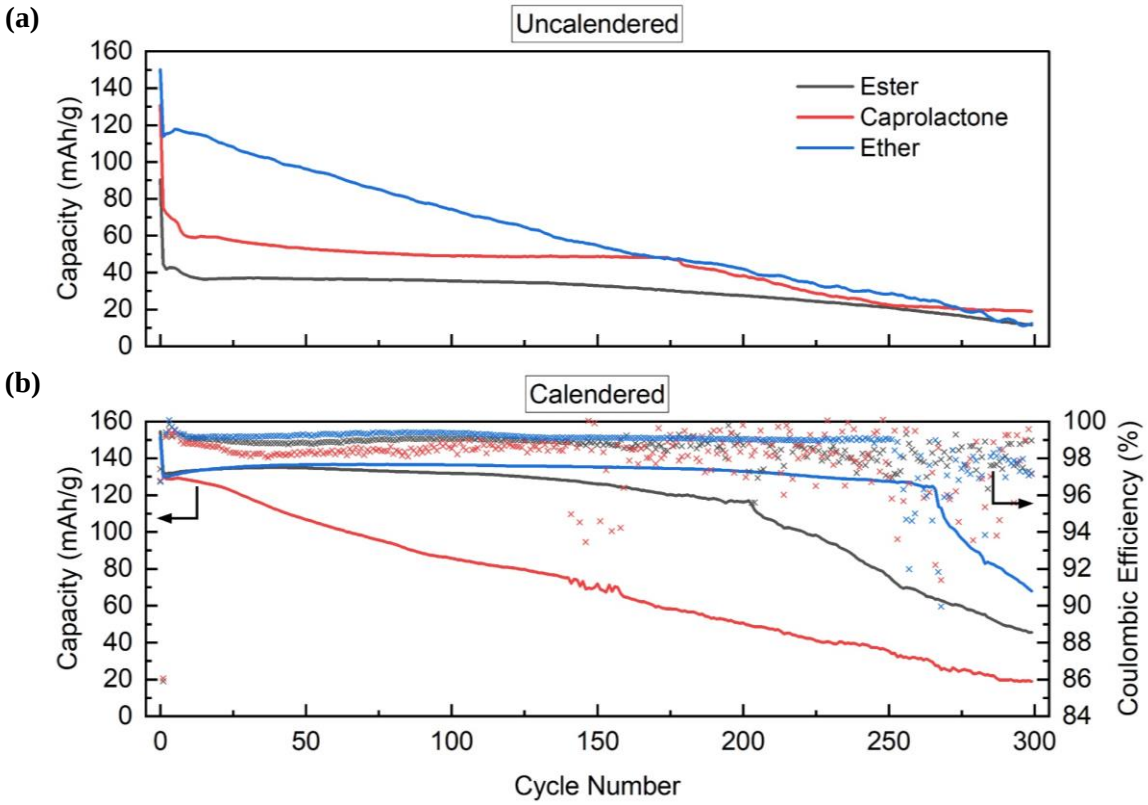

Figure 4. (a) Uncalendered and (b) calendered capacities of 90:5:5 PU chemistries when cycled at 0.5C/1C charge/discharge.

Table 3. PVDF and Ether-PU formulations tested.

Formulation Name	Abbreviation	LFP (wt%)	PVDF (wt%)	Ether-PU (wt%)	C65 (wt%)
PVDF 90:5:5	PVDF5	90	5		5
PU 90:5:5	PU5	90		5	5
PU 85:7.5:7.5	PU7.5	85		7.5	7.5
PU 80:10:10	PU10_10	80		10	10
PU 85:10:5	PU10_5	85		10	5

electrode/current collector interfacial area. The results for the calendered electrodes are displayed in Figure 4b. The process of calendering had a profound impact on both the caprolactone-PU and ester-PU electrodes, appearing to suppress the effects of swelling on the capacity. All three binders achieved capacities in excess of 130 mAh g^{-1} and the ether-PU and ester-PU had much improved cycling stability. The effects of calendering are complex as it is difficult to map the stress fields that develop in the composite microstructure. It is likely that the calendering process enhanced the electronic conductivity sufficiently beyond the percolation threshold, such that the subsequent conductivity drop due to swelling did not impair performance.[5] Hence, all three binders had similar initial capacities despite vastly different swelling susceptibility. However, the effects of swelling are still evident in the long-term cycling by the ether-PU having the best capacity retention and the ester-PU capacity dropping at a faster rate. The eventual capacity decay is not unusual in half-cell testing as the Li metal counter is prone to Li-ion depletion through Li plating, dendritic growth and side reactions.[23,24] The earlier onset for the ester-PU is consistent with a faster Li-ion depletion by the combined degradation at the cathode side.

The caprolactone-PU was not overly responsive to calendering, considering that it underwent less swelling than the ester-PU, with its performance expected to fall between the other two polymers. This deviation could have been the result of an older stock of coating being used, whereby coatings can degrade through ageing. Here a combination of long-term air exposure, resulting in lithium inventory loss, and water adsorption, causing hydrolysis of the polyurethane binder, can occur.[25,26]

To elucidate the impact of formulation on the electrochemistry, the ether-PU was tested at different binder and conductive additive loadings, shown in Table 3. It is evident in Figure 5 that at higher inactive material loadings the capacity improved. By testing formulations that contained dissimilar amounts of binder and conductive additive, it was clear that by increasing the conductive additive content the capacity could be maximised. These results reinforce the conclusion that the electrodes were limited by their electronic conductivity. The conductive additive content could be increased beyond 10% but this would have the negative consequences of a reduction in volumetric energy density since active material is lost in the process. Furthermore, all of the cycling data indicates that the

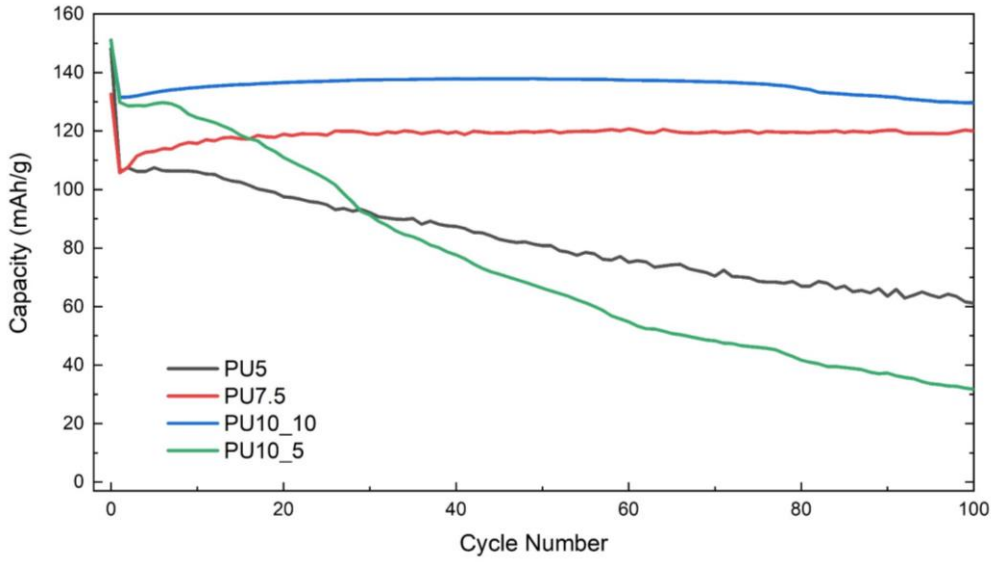

Figure 5. Capacity against cycle number for ether-PU formulations at 0.5C/1C charge/discharge cycling with 0.1C formation.

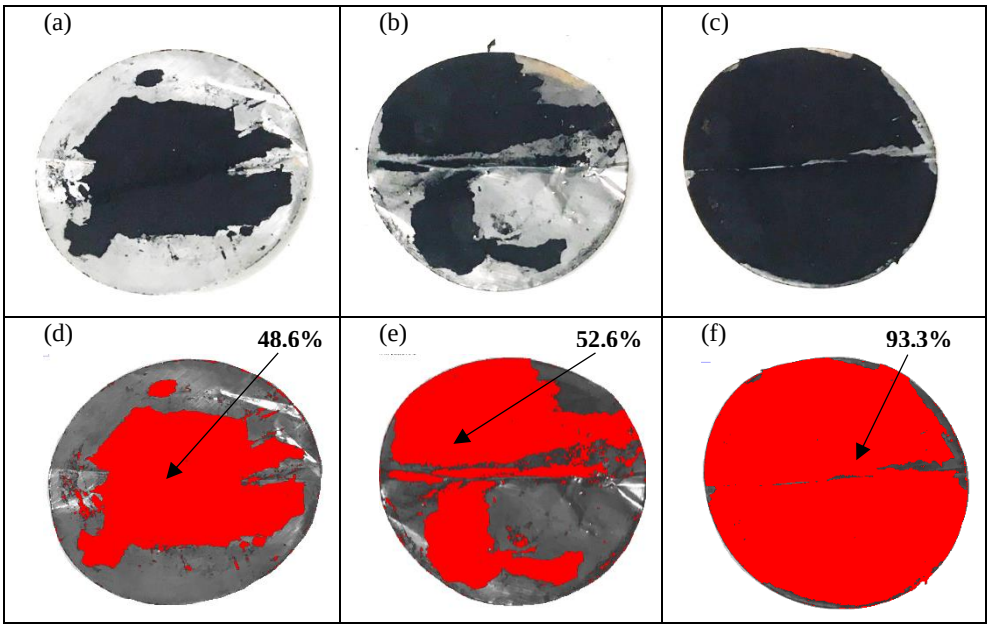

Figure 6. Post mortem (a) ester-PU, (b) caprolactone-PU and (c) ether-PU electrodes after creasing and (d – f) corresponding threshold maps of coating area.

active material has an upper capacity limit of 138 mAh/g at a 1C rate. Therefore any gains would be fractional and less than that sacrificed by the drop in active material content.

In summary, analysis of the electrochemistry shows that the high-swelling behaviour of ester-PU and caprolactone-PU compromises conductive pathways through interfacial delamination and expansion of the electrode. The swelling effects could be suppressed by calendering or mitigated by a higher content of conductive additive, enabling all three PU binders to attain specific capacities close to theoretical maximum. Calendering is preferable as it increases volumetric energy density by decreasing the thickness and avoids a reduction in active material content. However, for flexible batteries mechanical properties have a high priority and it is likely that a higher binder content will improve adhesion, cohesion and better accommodate stress. In order to increase binder content without compromising capacity, the conductive additive content also needs to be increased to provide sufficient conductivity. In other words, if flexible batteries are to benefit mechanically from a higher binder content they must balance this with a higher conductive additive content in order to retain low charge transfer resistance and thus maximise capacity.

Post-mortem analysis. The uncalendered electrodes (with 90:5:5 formulation) were removed from cells after cycling and folded completely in half in both directions to simulate extreme flexure. Figure 6 shows photos of the three PU electrodes after they have been folded, with the crease-line visible through the centre. Of the three binders, the ether-PU demonstrated the greatest area of coating retention on its surface, which appeared to be largely intact. Fracturing was evident along the crease-line

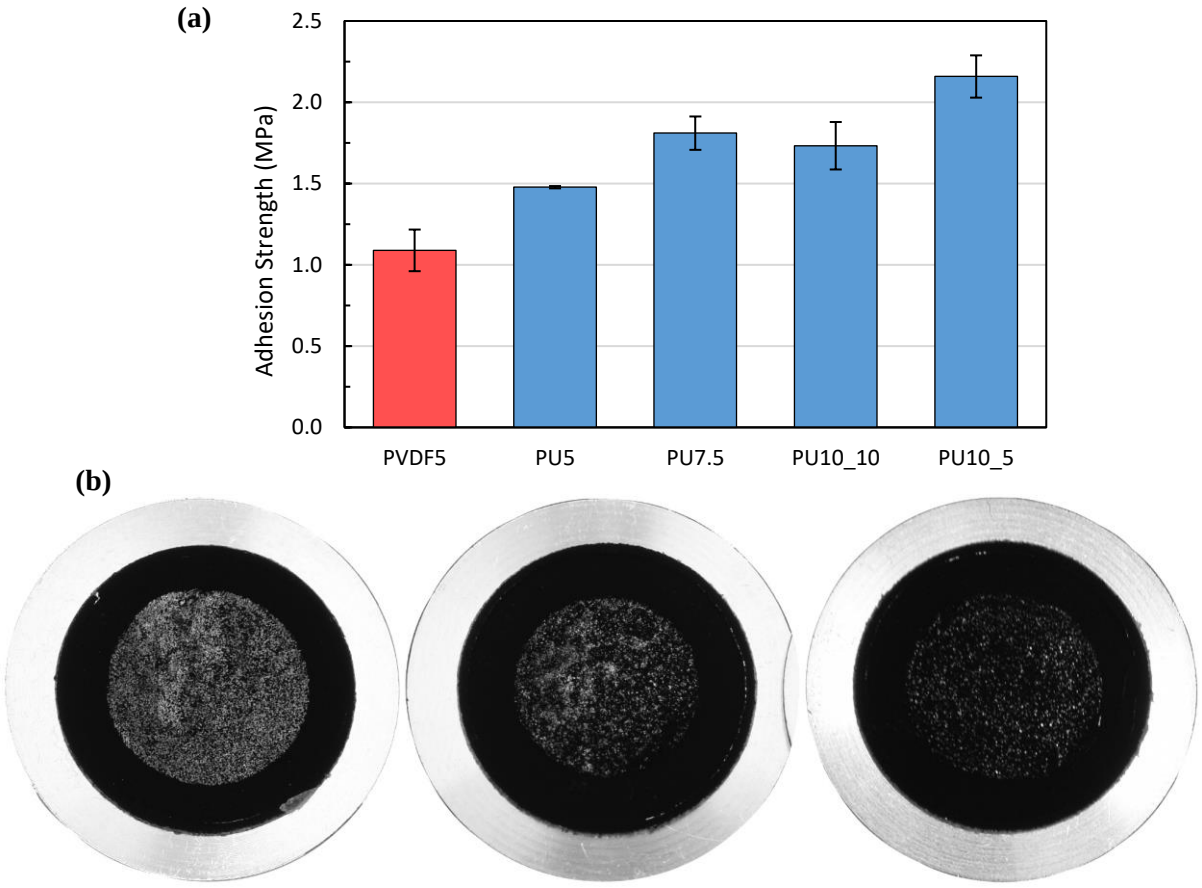

Figure 7. (a) Average (mean) adhesion strengths of ether-PU and PVDF formulations measured using pull-off adhesion test. A minimum of five specimens were tested for each formulation and the error bars show the 95% confidence interval. (b) Photographs of pull-off adhesion testing specimens after failure. From left to right, electrode formulations are PU5, PU7.5 and PU10_10.

with slight coating damage at the edges of the electrode. The caprolactone-PU and ester-PU binders suffered much greater damage, showing visible signs of coating delamination proximal to the folded areas. The images were analysed in an image-processing program (ImageJ) to quantify the percentage of coating that detached from the surface. The images were processed by applying a threshold filter and comparing the proportion of pixels that represented coating material with the total area of the electrodes. The results showed that the ester-PU lost the most material, with a 51.4% reduction in surface area, closely followed by the caprolactone-PU, with a 47.4% reduction. The ether-PU performed considerably better, losing only 6.7% of its coating. To corroborate these findings, the masses of the electrodes were recorded and compared to their masses prior to cell assembly. These comparisons confirmed the same trend with a 50.1% loss for the ester-PU and 44.2% for the caprolactone-PU.

It was evident from the post-mortem analysis that the binders which exhibited greater swelling and lower capacities also suffered more extensive damage when flexed. This reinforces the theory that swelling compromises binder/current collector and binder/particle interfaces. Weakened interfaces in coatings generally result in brittle composites that easily break apart when deformed. It seems promising then that the ether-PU swelled less than PVDF in common solvents.

Pull-off adhesion test. Pull-off adhesion testing of the electrodes was used to compare the adhesion strength of the ether-PU binder with PVDF. Delamination and cracking cause electrodes to fail when flexed. Strong adhesion to the current collector and cohesion between particles prevents disintegration, improves coulombic efficiency and prolongs cell cycle life. The formulations in Table 3 were tested by varying the binder and conductive additive content.

Comparing the PVDF5 and PU5 in Figure 7a, ether-PU adhesion strength was 35% higher than PVDF, showing clear improvement at identical loadings. By increasing binder content, adhesion could be improved further. At 10% binder content, the ether-PU had an adhesion strength twice that of the conventional PVDF electrode, showing that accepting small sacrifices in energy density can greatly benefit adhesion. The PU10_10 electrode exhibited a slight decrease in adhesion strength compared to the PU7.5 and PU10_5 electrodes. This can be attributed to the high specific surface area of the conductive additive compared with that of the active material. Increasing conductive additive content increases the total interfacial surface area. Assuming the binder coats the active material and conductive additive uniformly, the average thickness of the binder film decreases, which reduces the cohesion strength.[27]

The reduction in adhesion at higher conductive additive loadings, together with the need for sufficient conductive additive for electrical percolation of the conductive binder matrix, indicates that a binder content between 7.5% and 10% is more effective. It has been determined experimentally that when the conductive additive is between 5% and 7.5% adhesion is not generally compromised with standard binder loadings.

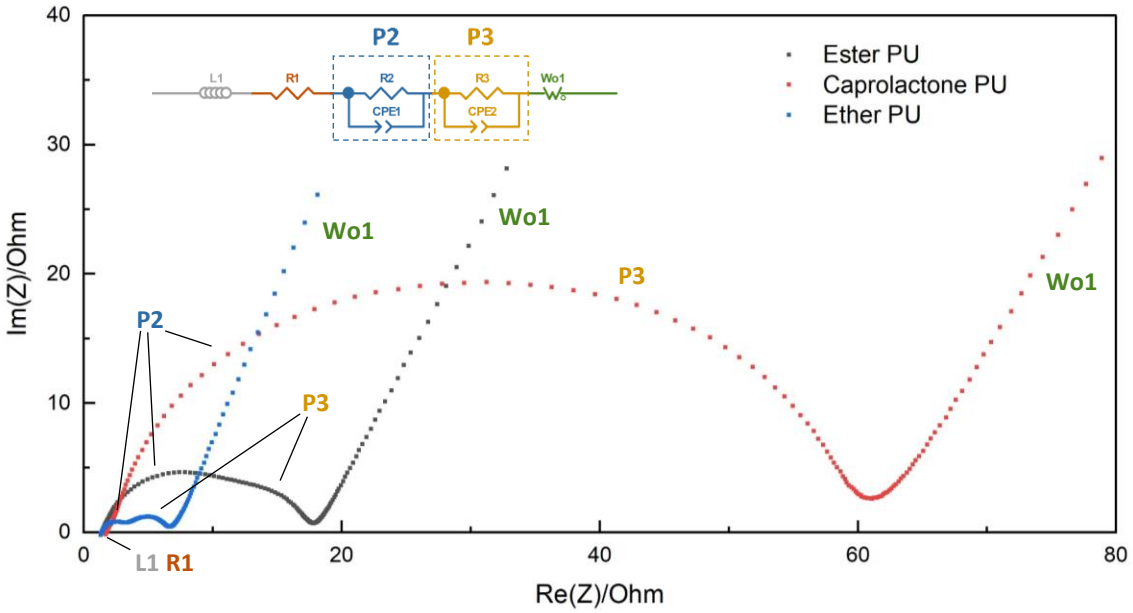

Figure 8. Nyquist plots for calendered PU electrodes after 10 charge/discharge cycles at 1C rate with labels showing equivalent circuit elements. Inset is equivalent circuit used to fit the impedance spectra.

An important feature of adhesion testing is the type of failure observed. Electrodes fail either adhesively, at the interface between the coating and the current collector, or cohesively, within the electrode coating. The type of failure indicates the weaker of the two interfaces. Electrodes of each of the three balanced PU formulations, after adhesion testing, are shown in Figure 7b. The density of lighter pixels indicates the tendency towards adhesive failure, as it shows a higher removal of particles from the surface. Almost all of the material was removed from the surface of the PU5 electrode, demonstrating adhesive failure, but the PU7.5 and PU10_10 electrodes had consecutively lower degrees of removal. This implied that at low binder and conductive additive loading the interface between coating and current collector was weakest. However, as their loadings were increased the interfaces within the coating became weakest. The electrode of formulation PU7.5 gave the highest adhesion strength, with neither adhesion nor cohesion as the dominant form of failure. Hence in Figure 7b it is observed at a transitional state where neither the majority of material is removed nor remains.

The adhesion results can be compared with the binder tensile properties to predict their respective modes of failure. It is clear that despite its low elastic limit, PVDF has a high yield strength (seen Figure 2). Therefore, it will elastically deform up to a higher maximum stress than the PU binders. On the outset this seems like an advantage for PVDF. However, consider the case where the cyclic strain is at a maximum of 5%. By multiplying this by the Young's modulus for each binder (see Table 2), the respective internal stresses can be elucidated.

For PVDF the internal stress is close to 40 MPa. This is lower than the failure stress of PVDF so initially the binder itself might cope with the strain but this means there will also be a similar level of stress on the adhesive interfaces in the composite. The adhesion strengths were quantified in Figure 7a and were found to be in the range of 1 – 2 MPa. As the adhesion strength of PVDF is an order of magnitude lower than 40 MPa, the stress transferred to the adhesive interface will cause it to fail. In its electrolyte-swollen state PVDF is documented as having a modulus five times lower than when dry.[28,29] Even though this will reduce the internal stress to 8 MPa, this is still far higher than the adhesion strength so the interface will fail irrespectively.

At the other extreme, the ester-PU and caprolactone-PU yield to internal stresses of just over 1 MPa at 5% cyclic strain. Assuming similar adhesion strengths to ether-PU, which in its worst case scenario was 1.5 MPa, the internal stresses do not exceed adhesion, such that the binder should remain adhered to the active electrode particles. However, the high swelling of these binders in the electrolyte will weaken their tensile properties, making them prone to irreversible internal damage. The ether-PU serves as an excellent compromise as at a 5% strain the ether-PU internal stress will be around 3.5 MPa. Therefore, assuming a five times reduction in strength due to swelling, in its swollen state it should experience internal stresses of 0.7 MPa which is lower than its adhesion strength. This serves to avoid adhesive failure and effectively accommodate bending stresses.

Potentiostatic Electrochemical Impedance Spectroscopy (PEIS). Electrochemical impedance spectroscopy (EIS) was used to identify the most prominent loss processes and quantify their individual contributions. Impedance analysis was carried out on the calendered 90:5:5 formulations for each PU binder. The electrochemical cycling and post-mortem studies indicated that a high degree of polymer swelling caused the binder to delaminate from both particle surfaces and the current collector. This was anticipated to manifest as a larger contact resistance between active material particles and the current collector for the high-swelling polymer chemistries, the ester-PU and caprolactone-PU.

Kramers-Kronig residuals were calculated to verify that the impedance response was consistent with a linear, stable and causal system (see Figure S3 in the Supporting Information). For the ether-PU (Figure S3A) the residuals (both real and imaginary parts) were below 0.5% for the entire frequency range which indicated high quality data. There was no prominent biasing towards either end of the frequency spectrum

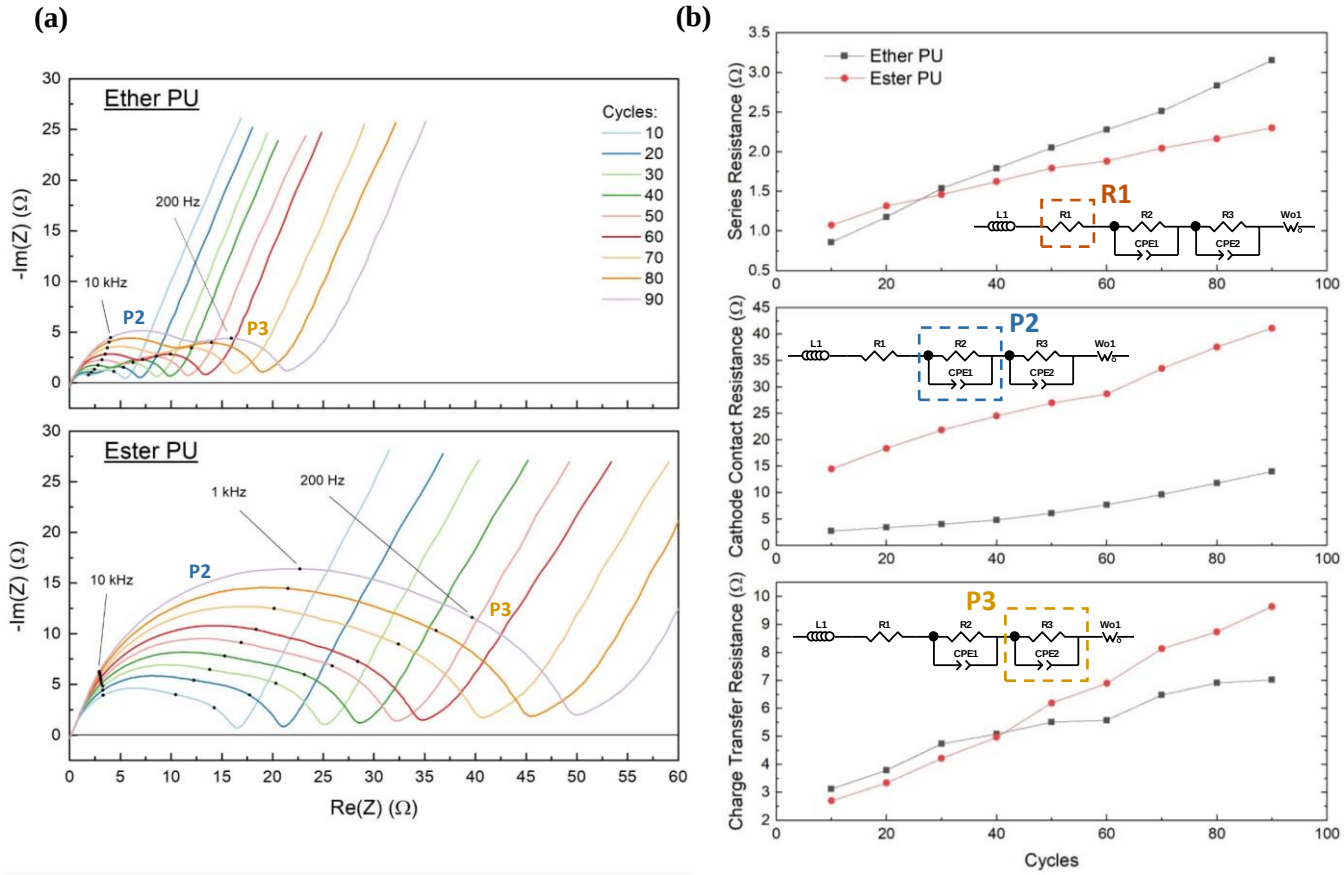

Figure 9. (a) Nyquist plots of calendered PU electrodes over duration of 90 charge/discharge cycles at 1C rate. (b) Series resistance, cathode contact resistance and charge transfer resistance of calendered PU electrodes from equivalent circuit fitting.

showing time invariance and a reliable measurement. For the ester-PU (Figure S3C) the residuals remained below 0.5% at almost all frequencies. There were only two points which were slight outliers (remained below 1%) and these occurred at high frequencies. The outliers were most likely artefacts of the high frequency measurement limitation of the potentiostat and are in the inductive region of the spectrum which is not a focus for this study. The residuals for the caprolactone-PU (Figure S3B) were very similar to the ester-PU. Therefore the ester-PU and caprolactone-PU impedance spectra are also valid for analysis.

A standard two-electrode system, with Li metal as the counter electrode, was used for EIS measurements. As it was a comparative study the absolute impedance values were not important and a three-electrode system would have been surplus to requirements. Using a two-electrode setup also avoided a change in cell geometry which can affect impedance values.

Observing the impedance spectra in Figure 8, there are two clearly distinguishable depressed semicircles in the ether-PU spectrum. The semicircles in the ester-PU and caprolactone-PU are harder to distinguish because of the higher impedance but the same reactions are present. These semicircles are represented by two RQ-elements in series in the equivalent circuit, denoted P2 and P3. An RQ-element consists of a resistor in parallel with a constant phase element. At the high frequency intercept with the real axis the imaginary impedance drops below zero indicating that there is inductance from the cabling or components. This is represented by an inductor and resistor in series in the equivalent circuit, denoted L1 and R1. The low frequency tail at 65 ° indicates diffusion processes. Deviation from ideal semi-infinite diffusion, seen as a 45 ° tail, are typically related to pore geometry. In this case the greater angle suggests pores which narrow along their length. The longer timescales of diffusion processes makes them sensitive to drift in voltage and current baselines. They are modelled with a Warburg element, denoted Wo1.

The impedance spectra for the calendered PU electrodes were recorded every 10 charge/discharge cycles at a 1C rate and the resultant Nyquist plots are shown for each PU chemistry in Figure 9a. The spectra were adjusted to pass through the origin and data below the x-axes were removed so that the evolution of P2 and P3 could be examined. As evident from Figure 8, the caprolactone-PU showed much greater impedance than the other two polymers. Due to the high impedance, there was significant shift in the characteristic frequencies and overlapping of semicircles making it difficult to distinguish the impedance processes. Therefore, the caprolactone PU impedance results were not used for detailed ageing analysis or equivalent circuit fitting. Their high impedance is likely to be linked to the same factors described in the calendering analysis regarding the coating age. Binder degradation weakened the binder/particle interfaces resulting in a higher contact resistance and increasing the susceptibility to swelling damage.

The lower frequency semicircle with a characteristic frequency of 200 Hz, labelled P3 in Figure 9a, is consistent with charge transfer processes and the solid electrolyte interphase (SEI) layer at the Li counter electrode, which occur between 100 Hz and 800 Hz in Li/Li symmetric cells.[30–32] The Li counter response is not relevant for full cells or binder performance and the variation between cells is mostly dependent on the surface morphology of the Li metal.[33] However, P3 also falls within the frequency range of cathode charge transfer resistance.[34,35] P3

evidently increases with swelling as it is significantly larger for the ester-PU and caprolactone-PU cells. Li metal defects are unlikely to contribute to this level of variation, so an increase in the cathode's collective charge transfer resistances is the most plausible cause. It is possible that as the binder swells it fills the voids in the electrode, reducing the porosity. Charge transfer resistance increases with porosity reduction as fewer charge transfer reaction sites are available.[36]

The semicircle with a characteristic frequency between 10 kHz and 1 kHz, labelled P2 in Figure 9a, is visible in both the ether-PU and ester-PU spectra. High frequency semicircles above 1 kHz are usually attributed to contact resistance between active material particles and current collectors.[30,37,38] They are sometimes attributed to the SEI layer but the low working voltage of LFP inhibits electrolyte decomposition and the Li metal SEI is observed at lower frequencies.[23,31] Therefore P2 is most likely to represent contact resistance between active material particles and current collectors.

The spectra were fitted to the equivalent circuit shown inset in Figure 8 using ZView software. The fitting enabled the series resistance (R1) and the contact resistance associated with P2 to be calculated. Their evolution with cycle number is shown in Figure 9b.

The series resistance (R1) predominantly originates from the state-of-health (SoH) of the electrolyte properties. R1 remained a similar magnitude for both polymers which was in line with expectations as identical electrolytes and cell geometries were used. R1 increased gradually with cycle number, consistent with normal electrolyte decomposition.

In both the ether-PU and ester-PU cells the fitting results show an increase in contact resistance as the number of cycles increase. However, the initial resistance is over four times higher in the ester-PU cell compared to the ether-PU and increases at a much faster rate. This is in accordance with their respective spectra, where P2 is much larger in the case of the ester-PU. The higher initial resistance in the ester-PU cell suggests a poorer electrical contact between the active material particles and the current collector. As equal proportions of conductive additive and consistent degrees of calendering are used for both electrodes, the large difference in resistance are likely to be related to contact area. The reduced contact area in the case of the ester-PU cell could be explained by the partial detachment of active particles from the current collector surface as a result of binder swelling. Similar transitions in the impedance spectra are recorded in the literature when LFP cathodes are calendered.[30] Calendering induces a frequency shift from 1 kHz to 10 kHz accompanied by a large drop in resistance. The transitions are explained by an increase in contact area between the active material particles and the current collector upon calendering. In this work calendering is fixed at 50% porosity, but it is logical that electrode expansion, caused by binder swelling, would see an opposite shift in the EIS to the compression induced by calendering. Hence, P2 shifts from 10 kHz to 1 kHz and the contact resistance increases when comparing the ester-PU to the ether-PU. The shift to lower frequencies with increasing impedance indicates that the timescales of conduction through these interfaces increases as they become more resistive.

In summary, the EIS results reinforce the theory that binder swelling compromises the interfacial integrity between the active material particles and the current collector. This is visible as an increase in contact resistance in Figure 9b for the ester-PU compared to the ether-PU. The charge transfer resistance also appears to increase with swelling which relates to a reduction in porosity. However, the charge transfer resistance only contributed to a small amount of additional resistance, as can be seen in Figure 9b. It was not possible to distinguish an increase in resistance between neighbouring active particle interfaces.

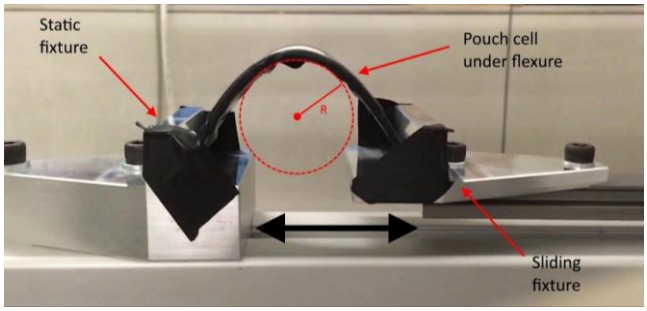

Figure 10. Pouch cell under flexure on custom-designed flexure rig. 'R' indicates the bending radius measurement.

Initial pouch cell flexure testing. Further research is underway to test and compare ether-PU with PVDF in a pouch cell environment. A custom-designed cell flexure rig has been constructed so that the pouch cells can be fatigue-flexed in conjunction with capacity and impedance analysis. Figure 10 shows a pouch cell under flexure on the testing rig.

CONCLUSIONS

This work has highlighted the significance of the binder choice and the interaction between binder and battery electrolyte solvents when selecting polymers for flexible batteries. In the presence of the electrolyte, the desirable mechanical properties of a binder can be jeopardised through excessive swelling. The reversible capacity and cycle life of the battery can then deteriorate through loss of interfacial contact and overall integrity of the electrode. This becomes especially important in the case of flexible batteries, where it is not only detrimental to the battery's electrochemistry but also to the supposed mechanical advantage of utilising tougher polymers as binders.

Previous reports have focused on the mechanical properties of binders prior to exposure to electrolyte but this is an unreliable way of predicting their performance without an accompanying understanding of how they interact with the electrolyte. During operation, binders are continually exposed to the electrolyte solvents and their mechanical properties are not necessarily retained over time, as evidenced by the PU binder chemistries studied in this work. It was shown that PU could effectively provide the functions of a conventional binder but when considering the toughness and adhesion required for enduring fatigue flexure, not all the chemistries were suitable. The PU chemistries that consisted of ester and caprolactone diol precursors were highly susceptible to swelling in the battery electrolyte solvents. The accompanying capacity loss could be suppressed by calendering, but the associated detriment to the mechanical properties proved irreversible. By comparison, the ether-based PU underwent less swelling than PVDF, retained good adhesion in the presence of the electrolyte and was consistently tougher and more durable. This makes it a highly promising candidate as a flexible battery binder.

In conclusion, when investigating binders for flexible batteries it remains important to measure the strength, toughness and adhesive capability prior to electrolyte exposure,

as this provides an initial indication of the binder's favourable properties. However, to predict real performance these tests must be supplemented with an understanding of the binder's behaviour in the electrolyte.

ASSOCIATED CONTENT

Supporting Information. Initial voltage against capacity profiles of PU chemistries; residuals calculated using Lin-KK software for impedance spectra of PU chemistries (PDF)
This material is available free of charge via the Internet at http://pubs.acs.org.

AUTHOR INFORMATION

Corresponding Author

*(C.A.J.) E-mail: c.jenkins.2@warwick.ac.uk

Author Contributions

C.A.J. performed the experiments and wrote the initial manuscript. S.R.C. and M.J.L. contributed their guidance and to manuscript revision. All authors have given approval to the final version of the manuscript.

ACKNOWLEDGMENTS

We gratefully acknowledge the support of HVM Catapult in providing access to equipment and materials.

REFERENCES

(1) Wen, L.; Li, F.; Cheng, H.-M. Carbon Nanotubes and Graphene for Flexible Electrochemical Energy Storage: From Materials to Devices. *Adv. Mater.* **2016**, *28* (22), 4306–4337. https://doi.org/10.1002/adma.201504225.

(2) Yuca, N.; Zhao, H.; Song, X.; Dogdu, M. F.; Yuan, W.; Fu, Y.; Battaglia, V. S.; Xiao, X.; Liu, G. A Systematic Investigation of Polymer Binder Flexibility on the Electrode Performance of Lithium-Ion Batteries. *ACS Appl. Mater. Interfaces* **2014**, *6* (19), 17111–17118. https://doi.org/10.1021/am504736y.

(3) Harris, K. D.; Elias, A. L.; Chung, H. J. Flexible Electronics under Strain: A Review of Mechanical Characterization and Durability Enhancement Strategies. *J. Mater. Sci.* **2016**, *51* (6), 2771–2805. https://doi.org/10.1007/s10853-015-9643-3.

(4) XYZTEC. Newsletter: Fracture strength of thin wafers and die https://www.xyztec.com/en/news/newsletter-30/Fracture-strength-of-thin-wafers-and-die.

(5) Liu, G.; Zheng, H.; Song, X.; Battaglia, V. S. Particles and Polymer Binder Interaction: A Controlling Factor in Lithium-Ion Electrode Performance. *J. Electrochem. Soc.* **2012**, *159* (3), A214–A221. https://doi.org/10.1149/2.024203jes.

(6) Yoshio, M.; Brodd, R. J.; Kozawa, A. *Lithium-Ion Batteries: Science and Technologies*; Springer Science: New York, 2009.

(7) Chen, H.; Ling, M.; Hencz, L.; Ling, H. Y.; Li, G.; Lin, Z.; Liu, G.; Zhang, S. Exploring Chemical, Mechanical, and Electrical Functionalities of Binders for Advanced Energy-Storage Devices. *Chem. Rev.* **2018**, *118* (18), 8936–8982. https://doi.org/10.1021/acs.chemrev.8b00241.

(8) Kim, Y. S. Interfacial Adhesion Mechanism between PVdF Binder and Copper Electroplate for Lithium Ion Secondary Batteries, Pohang University of Science and Technology, Pohang, 2000.

(9) Jurczuk, K.; Galeski, A.; Mackey, M.; Hiltner, A.; Baer, E. Orientation of PVDF α and γ Crystals in Nanolayered Films. *Colloid and Polymer Science*. 2015, pp 1289–1297. https://doi.org/10.1007/s00396-015-3542-7.

(10) Hencz, L.; Chen, H.; Ling, H. Y.; Wang, Y.; Lai, C.; Zhao, H.; Zhang, S. *Housing Sulfur in Polymer Composite Frameworks for Li–S Batteries*; Springer Berlin Heidelberg, 2019; Vol. 11. https://doi.org/10.1007/s40820-019-0249-1.

(11) Lee, Y. H.; Kim, J. S.; Noh, J.; Lee, I.; Kim, H. J.; Choi, S.; Seo, J.; Jeon, S.; Kim, T. S.; Lee, J. Y.; Choi, J. W. Wearable Textile Battery Rechargeable by Solar Energy. *Nano Lett.* **2013**, *13* (11), 5753–5761. https://doi.org/10.1021/nl403860k.

(12) Qi, H. J.; Boyce, M. C. Stress-Strain Behavior of Thermoplastic Polyurethanes. *Mech. Mater.* **2005**, *37* (8), 817–839. https://doi.org/10.1016/j.mechmat.2004.08.001.

(13) Park, G.; Park, Y.; Park, J.; Lee, J. Flexible and Wrinkle-Free Electrode Fabricated with Polyurethane Binder for Lithium-Ion Batteries. *RSC Adv.* **2017**, *7* (26), 16244–16252. https://doi.org/10.1039/C7RA00800G.

(14) Bao, J. J.; Zou, B. K.; Cheng, Q.; Huang, Y. P.; Wu, F.; Xu, G. W.; Chen, C. H. Flexible and Free-Standing LiFePO4/TPU/SP Cathode Membrane Prepared via Phase Separation Process for Lithium Ion Batteries. *J. Memb. Sci.* **2017**, *541* (April), 633–640. https://doi.org/10.1016/j.memsci.2017.06.083.

(15) Larsson, F.; Andersson, P.; Blomqvist, P.; Mellander, B. E. Toxic Fluoride Gas Emissions from Lithium-Ion Battery Fires. *Sci. Rep.* **2017**, *7* (1), 1–13. https://doi.org/10.1038/s41598-017-09784-z.

(16) Sigma Aldrich. Sigma Aldrich Polyurethane Product Properties https://www.sigmaaldrich.com/catalog/product/aldrich/430218?lang=en&region=GB (accessed May 4, 2020).

(17) BASF SE. Thermoplastic Polyurethane elastomers (TPU) https://www.basf.com/kr/documents/ko/product/Thermoplastis Polyurethan_Think, Create Elastollan.pdf.

(18) Haselrieder, W.; Westphal, B.; Bockholt, H.; Diener, A.; Höft, S.; Kwade, A. Measuring the Coating Adhesion Strength of Electrodes for Lithium-Ion Batteries. *Int. J. Adhes. Adhes.* **2015**, *60*, 1–8. https://doi.org/10.1016/j.ijadhadh.2015.03.002.

(19) Qian, G.; Liao, X.; Zhu, Y.; Pan, F.; Chen, X.; Yang, Y. Designing Flexible Lithium-Ion Batteries by Structural Engineering. *ACS Energy Lett.* **2019**, *4* (3), 690–701. https://doi.org/10.1021/acsenergylett.8b02496.

(20) Korthauer, R. *Lithium-Ion Batteries: Basics and Applications*; Springer: Berlin, 2018. https://doi.org/10.1007/978-3-662-53071-9.

(21) Foster, J. M.; Huang, X.; Jiang, M.; Chapman, S. J.; Protas, B.; Richardson, G. Causes of Binder Damage in Porous Battery Electrodes and Strategies to Prevent It. *J. Power Sources* **2017**, *350*, 140–151. https://doi.org/10.1016/j.jpowsour.2017.03.035.

(22) Chen, Z.; Christensen, L.; Dahn, J. R. Comparison of PVDF and PVDF-TFE-P as Binders for Electrode Materials Showing Large Volume Changes in Lithium-Ion Batteries. *J. Electrochem. Soc.* **2003**, *150* (8), A1073. https://doi.org/10.1149/1.1586922.

(23) Julien, C.; Mauger, A.; Vijh, A.; Zaghib, K. *Lithium Batteries*; 2016. https://doi.org/10.1007/978-3-319-19108-9.

(24) Xiao, J.; Li, Q.; Bi, Y.; Cai, M.; Dunn, B.; Glossmann, T.; Liu, J.; Osaka, T.; Sugiura, R.; Wu, B.; Yang, J.; Zhang, J. G.; Whittingham, M. S. Understanding and Applying Coulombic Efficiency in Lithium Metal Batteries. *Nat. Energy* **2020**. https://doi.org/10.1038/s41560-020-0648-z.

(25) Langklotz, U.; Schneider, M.; Michaelis, A. Water Uptake of Tape-Cast Cathodes for Lithium Ion Batteries. *J. Ceram. Sci. Technol.* **2013**, *4* (2), 69–76. https://doi.org/10.4416/JCST2012-00036.

(26) Martin, J. F.; Yamada, A.; Kobayashi, G.; Nishimura, S. I.; Kanno, R.; Guyomard, D.; Dupŕ, N. Air Exposure Effect on LiFePO 4. *Electrochem. Solid-State Lett.* **2008**, *11* (1). https://doi.org/10.1149/1.2801016.

(27) Gaikwad, A. M.; Arias, A. C. Understanding the Effects of Electrode Formulation on the Mechanical Strength of Composite Electrodes for Flexible Batteries. *ACS Appl. Mater. Interfaces* **2017**, *9* (7), 6390–6400. https://doi.org/10.1021/acsami.6b14719.

(28) Takahashi, K.; Higa, K.; Mair, S.; Chintapalli, M.; Balsara, N.; Srinivasan, V. Mechanical Degradation of Graphite/PVDF Composite Electrodes: A Model-Experimental Study. *J. Electrochem. Soc.* **2016**, *163* (3), A385–A395. https://doi.org/10.1149/2.0271603jes.

(29) Magasinski, A.; Zdyrko, B.; Kovalenko, I.; Hertzberg, B.; Burtovyy, R.; Huebner, C. F.; Fuller, T. F.; Luzinov, I.; Yushin, G. Toward Efficient Binders for Li-Ion Battery Si-Based Anodes: Polyacrylic Acid. *ACS Appl. Mater. Interfaces* **2010**, *2* (11), 3004–3010. https://doi.org/10.1021/am100871y.

(30) Illig, J.; Chrobak, T.; Klotz, D.; Ivers-Tiffée, E. Evaluation of the Rate Determining Processes for LiFePO 4 as Cathode Material in Lithium-Ion-Batteries . *ECS Trans.* **2019**, *33* (29), 3–15. https://doi.org/10.1149/1.3564865.

(31) Schmidt, J. P.; Chrobak, T.; Ender, M.; Illig, J.; Klotz, D.; Ivers-Tiffée, E. Studies on LiFePO4 as Cathode Material Using Impedance Spectroscopy. *J. Power Sources* **2011**, *196* (12),

5342–5348. https://doi.org/10.1016/j.jpowsour.2010.09.121.

(32) Ovejas, V. J.; Cuadras, A. Impedance Characterization of an LCO-NMC/Graphite Cell: Ohmic Conduction, Sei Transport and Charge-Transfer Phenomenon. *Batteries* **2018**, *4* (3). https://doi.org/10.3390/batteries4030043.

(33) Bieker, G.; Winter, M.; Bieker, P. Electrochemical in Situ Investigations of SEI and Dendrite Formation on the Lithium Metal Anode. *Phys. Chem. Chem. Phys.* **2015**, *17* (14), 8670–8679. https://doi.org/10.1039/c4cp05865h.

(34) Suarez-Hernandez, R.; Ramos-Sánchez, G.; Santos-Mendoza, I. O.; Guzmán-González, G.; González, I. A Graphical Approach for Identifying the Limiting Processes in Lithium-Ion Battery Cathode Using Electrochemical Impedance Spectroscopy. *J. Electrochem. Soc.* **2020**, *167* (10), 100529. https://doi.org/10.1149/1945-7111/ab95c7.

(35) Illig, J.; Ender, M.; Chrobak, T.; Schmidt, J. P.; Klotz, D.; Ivers-Tiffée, E. Separation of Charge Transfer and Contact Resistance in LiFePO 4 -Cathodes by Impedance Modeling . *J. Electrochem. Soc.* **2012**, *159* (7), A952–A960. https://doi.org/10.1149/2.030207jes.

(36) Zhang, Y.; Yang, Z.; Tian, C. Probing and Quantifying Cathode Charge Heterogeneity in Li Ion Batteries. *J. Mater. Chem. A* **2019**, *7* (41), 23628–23661. https://doi.org/10.1039/c9ta06977a.

(37) Waag, W.; Käbitz, S.; Sauer, D. U. Experimental Investigation of the Lithium-Ion Battery Impedance Characteristic at Various Conditions and Aging States and Its Influence on the Application. *Appl. Energy* **2013**, *102* (April 2016), 885–897. https://doi.org/10.1016/j.apenergy.2012.09.030.

(38) Li, Y.; Bettge, M.; Polzin, B.; Zhu, Y.; Balasubramanian, M.; Abraham, D. P. Understanding Long-Term Cycling Performance of Li 1.2 Ni 0.15 Mn 0.55 Co 0.1 O 2 –Graphite Lithium-Ion Cells. *J. Electrochem. Soc.* **2013**, *160* (5), A3006–A3019. https://doi.org/10.1149/2.002305jes.

Insert Table of Contents artwork here